Critical Current Distribution in Co-Doped $YBa_2Cu_3O_{7-x}$ Single Crystals

by

Amy L. Droegemeier

A project

submitted to

Oregon State University

in partial fulfillment of
the requirements for the
degree of

Master of Science

Completed March 4, 1999
Commencement June 1999

TABLE OF CONTENTS

ABSTRACT

Voltage-current (V-I) curves of a cobalt-doped $YBa_2Cu_3O_{7-x}$ sample have been measured in the temperature range 88.55 K to 89.55 K for magnetic fields less than 1 T. Critical current distributions (CCD's) have been obtained from this data and are compared to the CCD's of polycrystalline samples reported by Babić et al. We find that the CCD's of a single crystal are narrower than those for a polycrystalline sample, and that the cobalt doping has the effect of weakening pinning and thereby decreasing the critical current of the sample.

1. INTRODUCTION

Since the discovery of High Temperature Superconductors (HTSC's) by Bednorz and Mueller in 1986 [1], there has been a resurgence of studies and articles written about superconductivity. As all of the new HTSC's are Type II superconductors, the last twelve years have seen many papers written about the unique qualities of Type II superconductors. One of the most hotly debated topics in HTSC circles is what causes the particular voltage-current characteristics of the HTSC's. One possibility which has been explored for the low-T_C superconductors is that the superconductor has a distribution of critical currents that arises from the inhomogeneities in the sample. In 1967, Baixeras and Fournet developed a technique for deriving the critical current distribution (CCD) of a low-T_C superconducting sample [2]. In this work we use this technique, which was quite successful in explaining the $V - I$ curves of composite superconductors, to explore the CCD's of a single crystal of $YBCO$. We find that this distribution is dependent on the applied magnetic field, the temperature and the microstructure of the sample. This technique can also give insight into the overall quality of the sample.

2. THEORY

2.1. Brief Theoretical Backdrop

Superconductors are materials which exhibit no electrical resistance to DC currents at sufficiently low temperatures. The temperature which separates the superconducting phase of a material from the normal phase is called the critical temperature, or T_c. There are two types of superconductors, appropriately named Type I and Type II. Both types exhibit the effect of zero resistance when cooled below their critical temperature. Their differences are manifest when the superconductors are placed in a magnetic field.

When a Type I superconductor is placed in a magnetic field, the critical temperature decreases as the strength of the magnetic field is increased. When the magnitude of the magnetic field exceeds a certain value known as the critical field, or H_c, the material behaves like a normal conductor with a finite resistance.

A peculiar effect discovered by W. Hans Meissner and Robert Oschenfeld in 1933 [3] can be observed when the superconductor is placed in a magnetic field while above T_c, and then cooled down below T_c. In a normal conductor the field would remain trapped in the interior of the material even after the field was removed. In a Type I superconductor, however, the flux is excluded from the interior of the material provided the field is below H_c.

Type II superconductors are characterized by two critical magnetic fields, H_{c1} and H_{c2}. Below H_{c1} the superconductor behaves like a Type I superconductor exhibiting zero resistance and flux exclusion. Above H_{c2} the material becomes normal again and displays complete flux penetration and an electrical resistance.

In between these two transition points is what is known as the mixed state, or vortex state, where it is energetically favorable to have many boundaries between the normal and superconducting states. The superconductor is penetrated by quantized flux

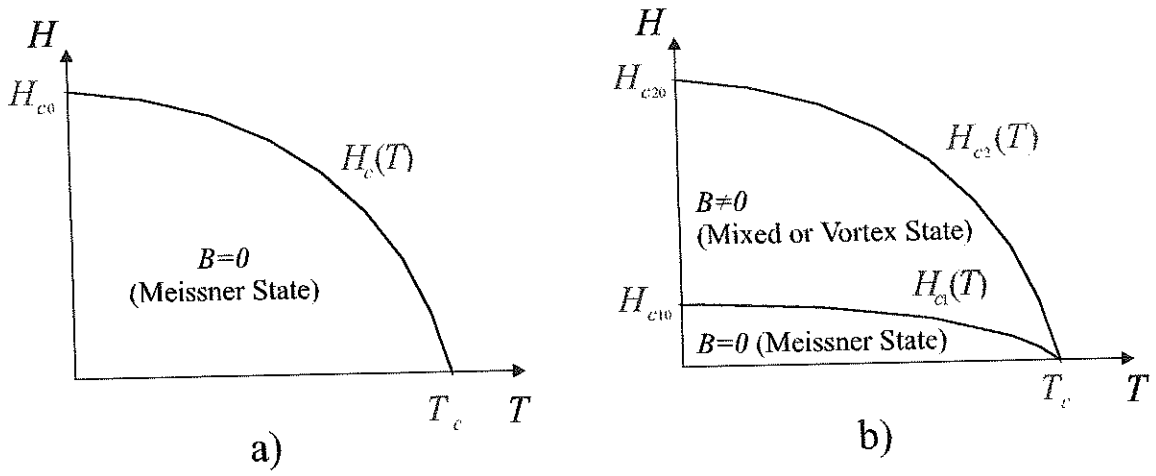

FIGURE 2.1. Phase Diagram for a) Type I superconductor, b) Type II superconductor.

tubes of normal matter, called vortices, and thus no longer exhibits perfect diamagnetism. A representative magnetic phase diagram for a Type I superconductor (fig. 2.1a) and a Type II superconductor (fig. 2.1b) is shown.

2.2. Vortex State

Understanding the nature of the mixed state is essential for a complete description of superconductivity. We will begin by looking at the vortex state of an ideal sample of a Type II superconductor.

2.2.1. Ideal Sample

When a transport current is applied to a Type II superconductor in the mixed state, the vortices which penetrate the sample will begin to move, driven by a Lorentz force

$$\vec{F} = \vec{J} \times \vec{B}$$

where $\vec{J}$ is the applied current, and $\vec{B}$ is the internal magnetic field. The motion is in a direction perpendicular to both the applied magnetic field and the applied current. This situation is depicted in figure 2.2.

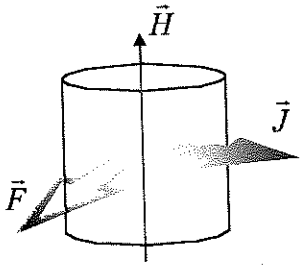

FIGURE 2.2. Schematic showing direction of applied current, $\vec{J}$, applied magnetic field, $\vec{H}$, and Lorentz force, $\vec{F}$.

This vortex motion is troublesome because flux flow causes power dissipation and electrical resistance in the crystal. As the flux moves through the sample, it gives rise to an electric field which is parallel to $\vec{J}$:

$$\vec{E} = \vec{B} \times \vec{v},$$

where $\vec{v}$ is the velocity of the flux. This field is obtained experimentally by measuring the voltage. By knowing the current applied we can determine the resistance of the sample.

In an ideal superconductor the vortices would move unimpeded for any value of applied current. This would render the mixed state impractical for any technological uses. In practice, however, defects in the sample can effectively pin the vortices and prevent them from moving.

2.2.2. Non-Ideal Sample

The inhomogeneities in superconducting materials which inhibit vortex motion are known as pinning sites or pins. These pinning sites can be viewed as potential energy wells [4] with a force of

$$\vec{F}_p = -\nabla U$$

A vortex which is trapped by one of these pinning sites is said to be pinned. Vortices which are not actually constrained by a particular pinning site can instead be limited by intervortex interactions which act to prevent the motion of the vortex array. Consequently, the Lorentz force exerted on a vortex by an applied current not only has to exceed the pinning force of the defect but also the force of the vortex interactions in order for the vortex to move.

The current at which vortices become depinned is known as the critical current, I_c. The critical current, like the critical magnetic field, increases as the temperature is lowered. A phase diagram showing the relationship between critical field, critical current, and critical temperature is shown below (fig. 2.3). The sample is superconducting only in the shaded portion of the diagram.

2.2.3. V-I Curves

There has been much effort put into understanding the voltage-current (V-I) characteristics of high-temperature superconductors. It has been found empirically that for the low current regions of the resistive transition, the shape of the V-I curve can be described by the power law $V \propto I^n$ [5–7]. In figure 2.4 a typical V-I curve for the sample in this study is shown in terms of the electric field density, $\vec{E}$, and critical current density,

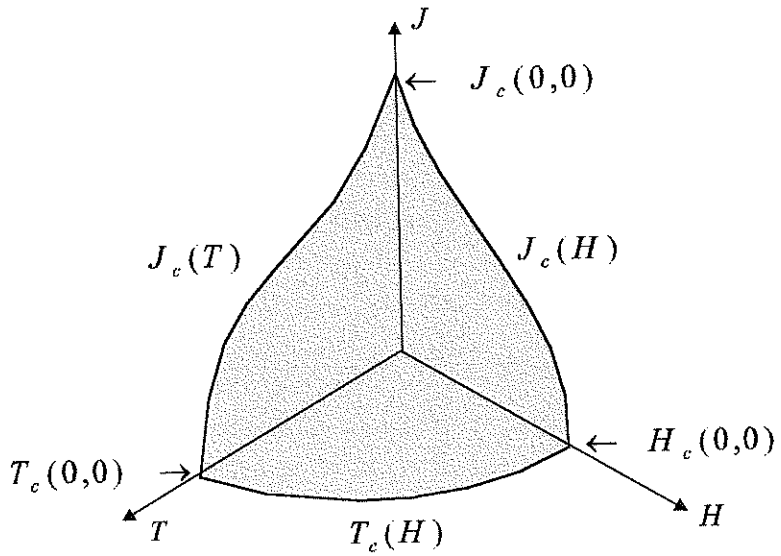

FIGURE 2.3. Three-dimensional phase diagram showing the relationship between critical current, critical field and critical temperature.

$\vec{J}$. The solid line is a $E \propto J^n$ fit for the E-J data below a certain value of J known as $< J_c >$, which will be defined later.

The origins of the shape of the E-J curve are currently being hotly debated in the high-T_c community [8, 9]. There are many different processes which can affect the curvature of the resistive transition. One explanation, more common in low-T_c circles, is that it is caused by flux creep [10–12]. Vortex motion above J_c, which has been discussed above, is known as flux flow. This type of motion is due to the Lorentz force of the applied current overcoming the pinning force of the defect sites. At currents smaller than J_c, however, vortices can become depinned due to thermal fluctuations. This thermally activated flux motion is known as flux creep. At sufficiently low currents, flux creep proceeds at an orderly pace and the amount of heat generated by it is not enough to be of practical importance. However, the average pinning force decreases exponentially as

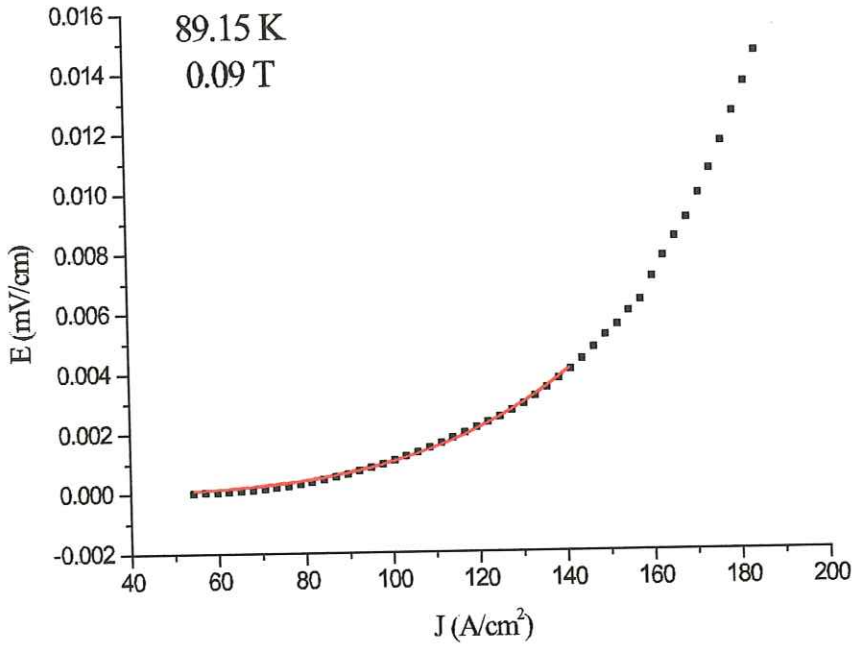

FIGURE 2.4. E-J curve for the sample at 89.15 K under a 0.09 T field. The solid curve shows a $E \propto J^n$ $(n = 4.02)$ fit for the data below $< J_c >$.

the temperature increases. At currents near the critical current the creep rate can build up suddenly to the point where a flux jump, or an avalanche of vortices occurs. These bundles of flowing vortices can produce enough heat to cause a localized return to the normal state [13]. The effects of flux creep, which introduces uncertainty into the value of J_c at any point in the sample, have been studied by Tinkham [11] and Soulen [12].

One of the more popular theories for the curvature among high-T_c researchers is a second-order phase transition between a vortex glass and a vortex liquid state [14, 15]. This theory predicts that E-J curves within the critical region can be collapsed into two universal curves, $E+$ and $E-$, with universal critical exponents ν and z. These universal functions should be independent of the material system [9]. Although the vortex glass theory has had quite a bit of recent success [14], especially in the high field region of the

phase diagram, it is not clear that it is the correct theory at lower fields. Here we will focus on a more conventional view of the resistive transition to see if it is adequate to explain the features without invoking more exotic theories.

2.3. Critical Current Distributions

In 1967, Baixeras and Fournet modeled the effects of critical-current inhomogeneity in a low-T_c Type II superconductor [2]. In this work, they developed a method for deriving the critical current distribution by taking the second derivative of the V-I data. Others have used this formalism to study the intrinsic and extrinsic limitations on the critical current density of $Nb-Ti$ and $NbSn_3$ composites [5, 6], and to study the decoupling of superconducting grains in high-T_c ceramics [7, 16].

This paper will attempt to explore the distribution of critical currents in an $YBa_2(Cu_{.99}Co_{.01})_3O_{7-x}$ single crystal using the method developed by Baixeras and Fournet. We begin formulating the technique by placing the sample in an external magnetic field between H_{c1} and H_{c2}, at a given temperature below T_c. We assume that the sample can be divided into different regions with different critical currents, with a maximum critical current of I_{cmax}. The reasons for the differences in critical current are debatable, (grain size, defect density, filament sausaging or surface defects) but for the purposes of the model it is not important and the portions of the sample with an I_c less than I_{cmax} are simply called weak links. We let there be a continuous distribution of critical currents throughout the sample. This distribution can be described by a normalized distribution function, $f(I_c)$:

$$\int_0^\infty f(I_c)dI_c = 1$$

The average value of the critical current can be found from:

$$< I_c >= \int_0^\infty I_c f(I_c)dI_c$$

The voltage across the sample is then:

$$V = R\int_0^\infty I_c f(I_c) dI_c$$

We can further simplify this equation by realizing that only the pinning sites with critical currents below the applied current I contribute to the losses in the sample. Equivalently, only the current above the critical current of each weak link will contribute to the power dissipation. As long as the applied current is less than the critical current at every point, the sample carries the current losslessly. We can now write the above equation as:

$$V = R\int_0^I (I - I_c) f(I_c) dI_c$$

In terms of electric field and critical current density, this is:

$$E = \rho\int_0^J (J - J_c) f(J_c) dJ_c$$

To obtain the distribution of critical currents in the sample, one solves for $f(J_c)$ by differentiating $E(J)$ with respect to J. Using Leibnitz' rule for differentiating integrals we obtain

$$\frac{dE(J)}{dJ} = \rho\int_0^J f(J_c) dJ_c$$

and upon differentiating again we get

$$\frac{d^2E(J)}{dJ^2} = \rho f(J_c)$$

Thus, the distribution of critical currents in the sample is obtained from the second derivative of the experimental $E(J)$ data with a proportionality of ρ. In the high-current limit the voltage can be written as

$$E(J) = \rho(J - < J_c >), \qquad J > J_{cmax} \tag{2.1}$$

where $< J_c >$ is the average critical current density with respect to the distribution $f(J_c)$,

$$< J_c >= \int_0^\infty J_c f(J_c) dJ_c$$

From equation 2.1 we see that the average critical current density can be found by extrapolating the linear part of the slope to zero field. In figure 2.5, the $V(I)$ curve of the sample under study is shown for 89.15 K in a .09 T field. The average J_c is shown, derived from the linear extrapolation.

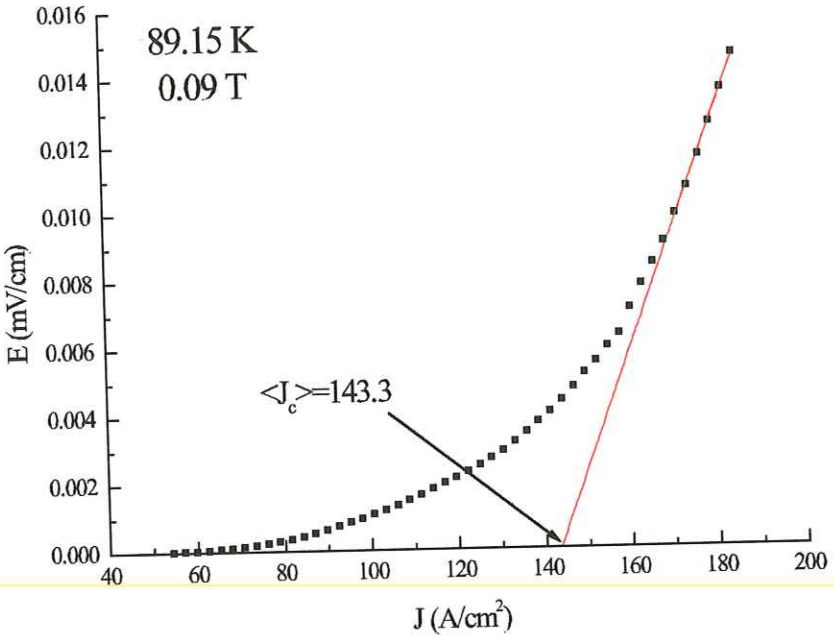

FIGURE 2.5. V-I curve for the sample at 89.15 K under a 0.09 T field. The solid line shows the linear extrapolation of the data to $E = 0$.

Because the transition from the flux-pinning, zero-resistance state to the flux-flow, resistive state occurs over a range of currents, it is difficult to accurately identify the intrinsic critical current of a sample. There have been many definitions used for the critical current, all of which generate different values for I_c [17, 18, 5]. One common definition typically used by magnet designers is the constant resistivity criterion I_{cr}, of $10^{-12}\ \Omega \cdot cm$. Flux pinning investigators generally adopt the constant voltage criterion, I_{cv} of 1 $\mu V/cm$ [17]. Dorofejev notes another definition as being I_{cq}, the current at which

quench occurs [18]. In this work we will use the average critical current, $< I_c >$, which we derived above, and the most common critical current, I_{cc}, which is defined as the current for which the distribution has its maximum value.

3. EXPERIMENT

3.1. Sample

The sample used in this experiment was a twinned $YBa_2(Cu_{.99}Co_{.01})_3O_{7-x}$ crystal on loan from Professor Ginsberg of the University of Illinois at Urbana-Champaign. The zero-field T_c of the sample, as determined from a resistivity measurement, was $\sim 91.2\ K$ with a transition width of $0.2\ K$ (see figure 3.1). The dimensions of the crystal were: $0.42 \times 0.44 \times .04\ mm^3$. The crystal was in the shape of a platelet, with the c-axis along the thin direction and the a-b planes forming the plate.

3.2. Experimental Setup and Data Collection

The original intent was to make contacts to the crystal in a four-point probe geometry, collect E-J data, remove the contacts, irradiate the crystal, remake the contacts and take data again. However, due to the small size of the crystal, making the contacts turned out to be a difficult task and in the process the crystal was broken in half. So we instead decided to use one half for the unirradiated experiment, and the other half for the irradiated experiment. Unfortunately, after excessive handling and the degradation due to irradiation, it was impossible to make the contacts for the second half. Therefore, this work will only study the CCD curves of the unirradiated portion of the crystal, and the results will be compared to similar studies done by Babić et al. on sintered ceramics [7].

The V-I data was collected using a standard four-point probe technique. This technique allows us to measure only the voltage drop across the sample and thus eliminate from the equation any resistance in the wires or contacts. The current was applied using a Keithley 220 current source and the voltage was measured using a Keithely 182 digital voltmeter. A schematic of the sample and contacts is shown in figure 3.2.

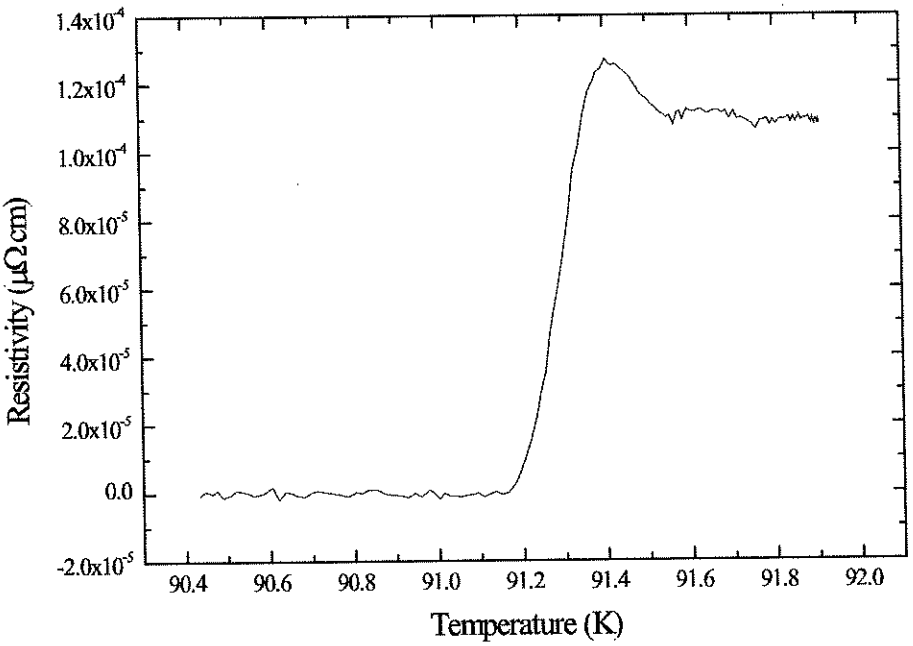

FIGURE 3.1. Temperature dependence of resistivity of sample at zero Tesla.

The basic process used for making the contacts was to attach the crystal to an MgO substrate for easier handling, and then use gold wire to paint onto the crystal four thin strips of conductive epoxy which served as bond pads. After curing the bond pads on, the actual contacts were made with gold wire. The reader is referred to the Ph.D. thesis of Brandon R. Brown [19] for a more detailed explanation of the method. The main difference between his method and this one was that we used a nonconductive epoxy (Duralco 4400) for attaching the crystal to the substrate.

With the crystal securely attached to the substrate and the wires bonded to the crystal, the whole setup was placed in a sample holder, which was designed and made in-house by Brandon Brown. The sample holder has a small pocket which, when layered

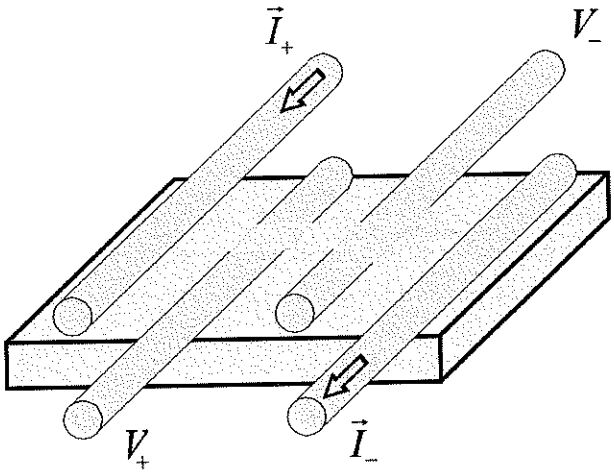

FIGURE 3.2. Schematic of sample with contacts for four-point probe.

with a tiny bit of silly putty[1], holds the substrate securely in place. The wires were then soldered to gold pads which run to gold pins for connection to the instruments. A photo of the setup is shown in figure 3.3.

Since much of the data was collected in the flux flow regime, it was crucial to have precise temperature control and stability. This was accomplished by using both hardware and software control. For the hardware control, the sample was placed in a liquid helium dewar with a variable temperature insert (VTI). The dewar consists of two chambers. The outer chamber is an insulating jacket filled with liquid nitrogen, and the inner one is kept filled with liquid helium. The VTI fits inside the inner chamber, and it is here that the sample is kept under a vacuum. The VTI contains a valve which allows liquid helium to seep in, and a heater, controlled by a DRC-91CA temperature controller, which regulates the temperature of the helium. Thus it is possible to have precise control over the temperature of the helium in the VTI. However, once a current was applied which

[1]next to duct tape, the most useful tool in a lab.

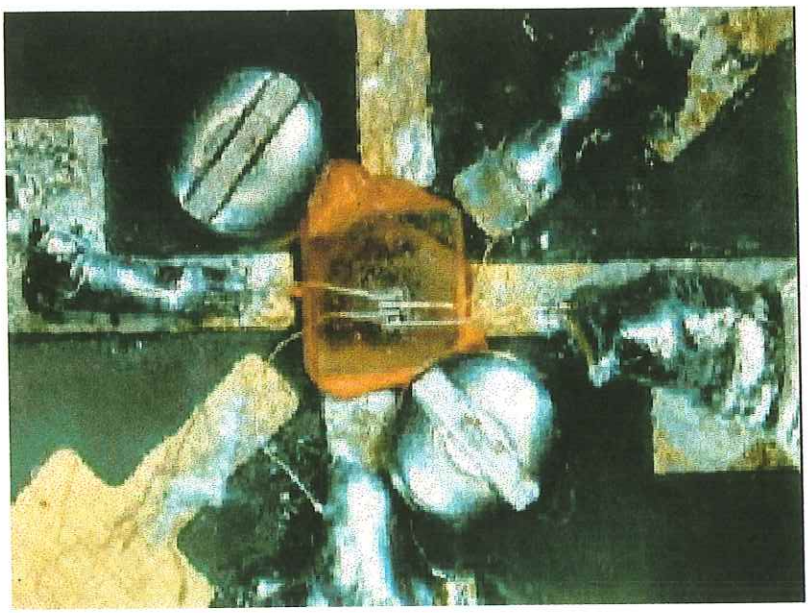

FIGURE 3.3. Photo of crystal on sample holder.

caused the crystal to have some resistance, the sample would begin to heat up due to power dissipation. Hence, it was necessary to wait a few seconds between data points to allow the sample to cool back down to the appropriate temperature. If the temperature began to drift, data collection was stopped until the temperature restabilized. This was accomplished by programming a waiting period and a stop button into the data collection routine.

The magnetic field was created by a 9 T $NbSn$ superconducting magnet. By varying the current through the magnet we were able to precisely control the field.

3.3. Irradiation

The other half of the crystal was sent to be irradiated at the University of Missouri Research Reactor. It was subjected to three hours of neutron irradiation with a flux of $8.000 \times 10^{13}\ n/(cm^2 \cdot sec)$. When returned it was too fragile to place the leads on it

it so the second half of the experiment was abandoned. A magnetization measurement was attempted to determine the T_c of the sample, but there was no detectable signal of superconductivity at 77 K.

4. RESULTS AND DISCUSSION

4.1. Results

The $E - J$ isotherms are presented first. Figures 4.1 - 4.3 show the log-log plot of E vs J for five different temperatures. The log-log plot is a useful form for plotting the data as it allows us to quickly determine if the data can be easily fit to a $E \propto J^n$ power law. The more linear the log-log data, the better the fit. As can be seen, the data fits to a power law quite well for higher fields ($> 0.2\ T$), and for lower fields the data is linear only in the low-current region. The n-value for the fit is therefore determined from the data below the average critical current $< J_c >$ for each set of data. The insets in the figures show the dependence of the power-law-fit exponent n on the magnetic field. One can see that the value of n decreases very rapidly for small fields. The exponent n is a

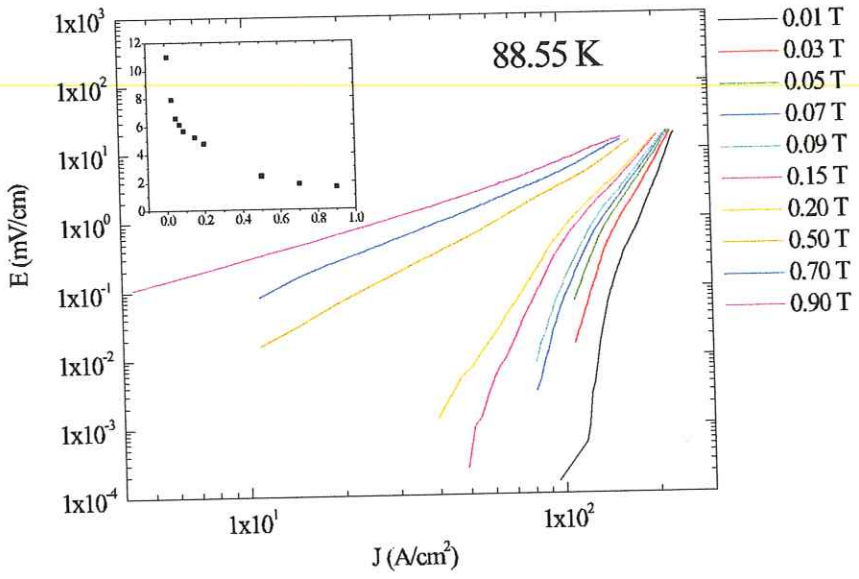

FIGURE 4.1. Electric Field vs. Current Density at 88.55 K. Inset shows dependence of parameter n on magnetic field.

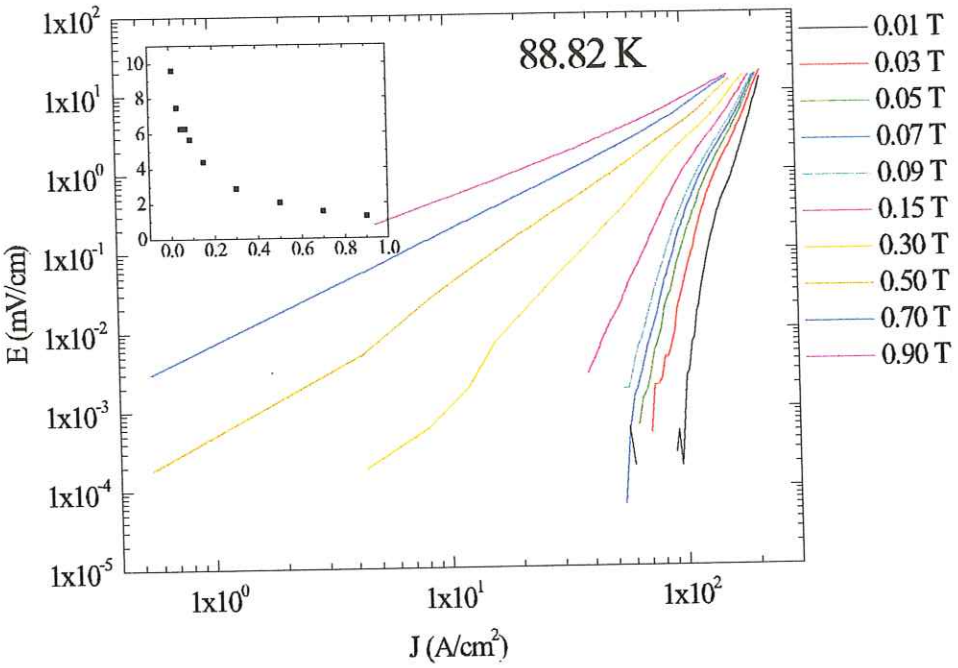

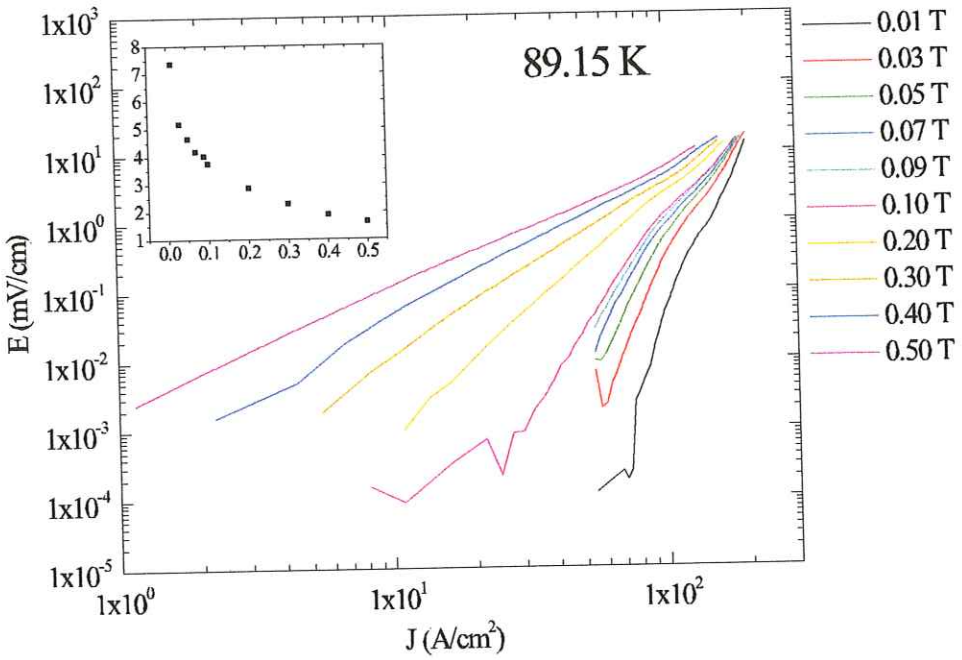

FIGURE 4.2. Electric Field vs. Current Density at 88.82 K and 89.15 K. Insets show dependence of parameter n on magnetic field.

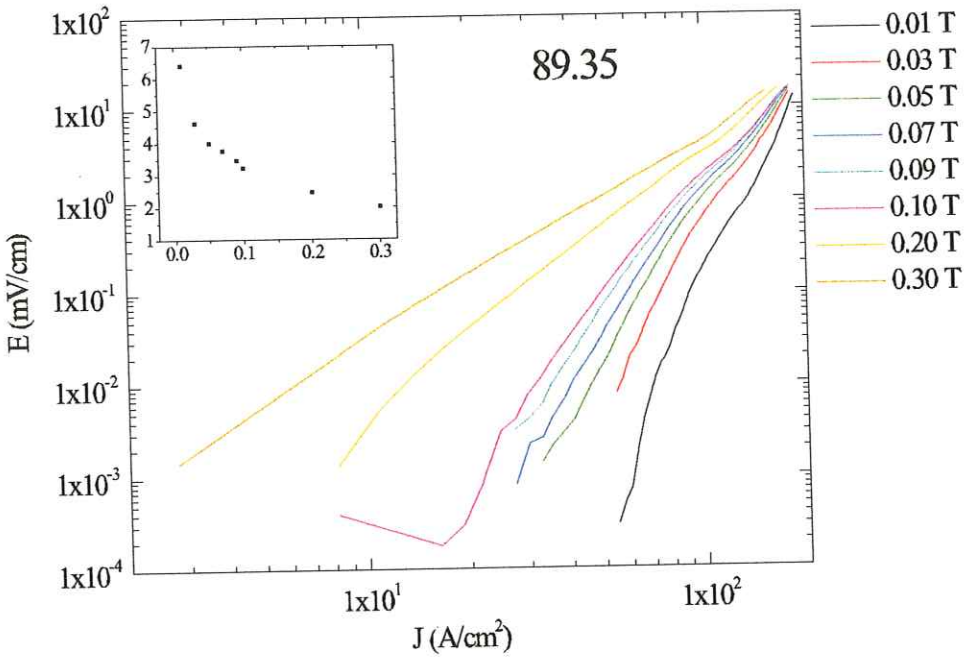

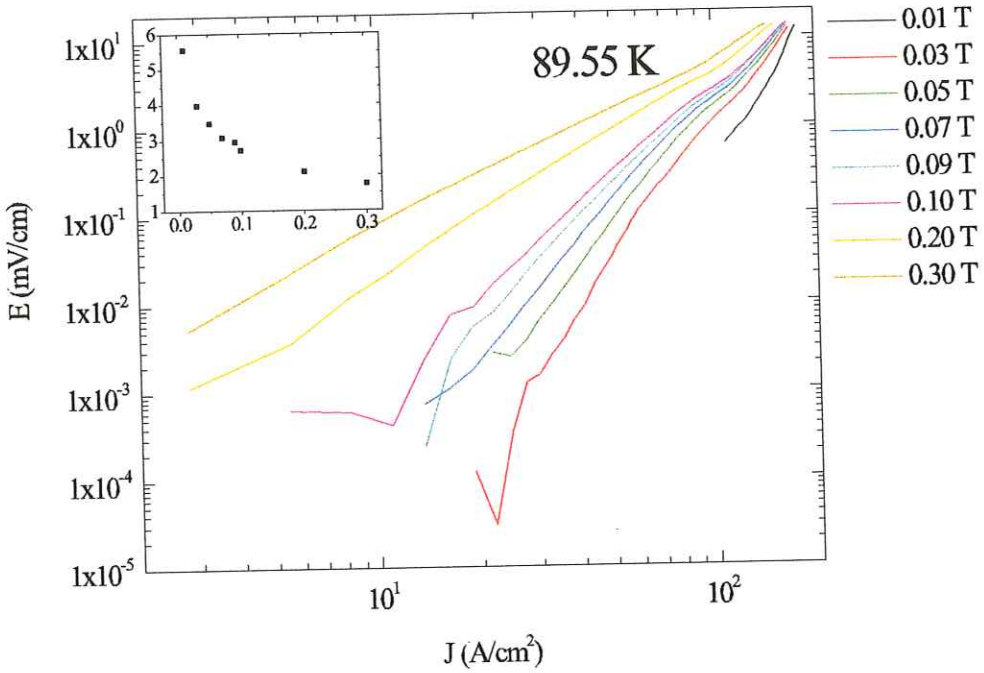

FIGURE 4.3. Electric Field vs. Current Density at 89.35 K and 89.55 K. Insets show dependence of parameter n on magnetic field.

measure of the sharpness of the resistive transition, and the decrease in n can be roughly correlated to a broadening of the critical current distributions.

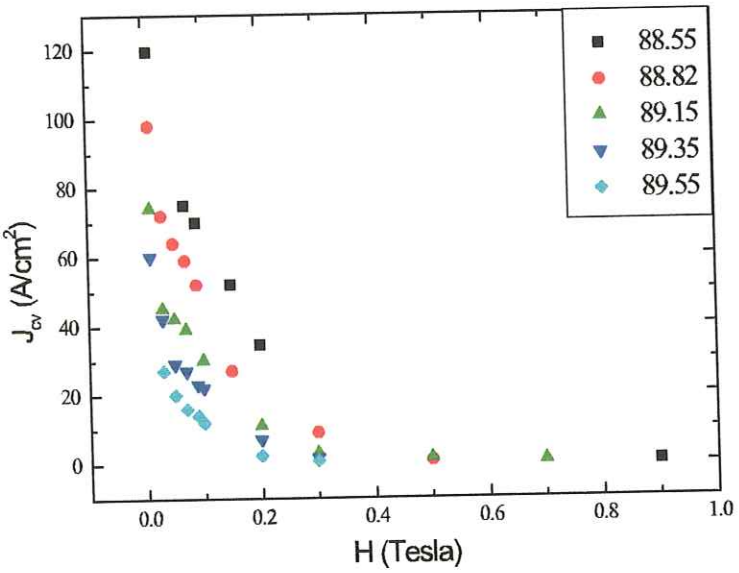

FIGURE 4.4. Constant-voltage critical current vs. magnetic field at several temperatures.

A conventional analysis of $E - J$ data would find the J_{cv} of the sample by using a constant voltage criterion. This has been done, and plots of J_{cv} vs. magnetic field are shown in fig. 4.4. Some of the $E - J$ data collection was begun at a current already above the conventional J_c of 1 $\mu\ V/cm$, and therefore the data was extrapolated from the $E \propto J^n$ fit. One can see from the plot that for low fields the J_{cv} decreases very rapidly with increasing field and appears to be temperature independent above about 0.3 T. In contrast, the $< J_c >$(fig. 4.5) and the J_{cc}(fig. 4.6) calculated from the CCD's remain dependent on temperature up to at least 0.5 T (possibly higher). Of note is the fact that the J_{cv}, which is the standard criterion for determining J_c in flux-pinning investigations, is between 80 and 150 A/cm^2 lower than the current at the peak of the distribution.

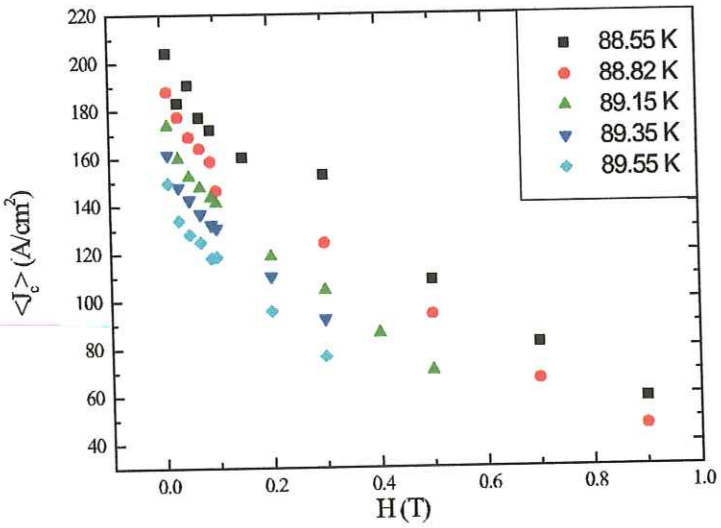

FIGURE 4.5. Average critical current vs. magnetic field at several temperatures.

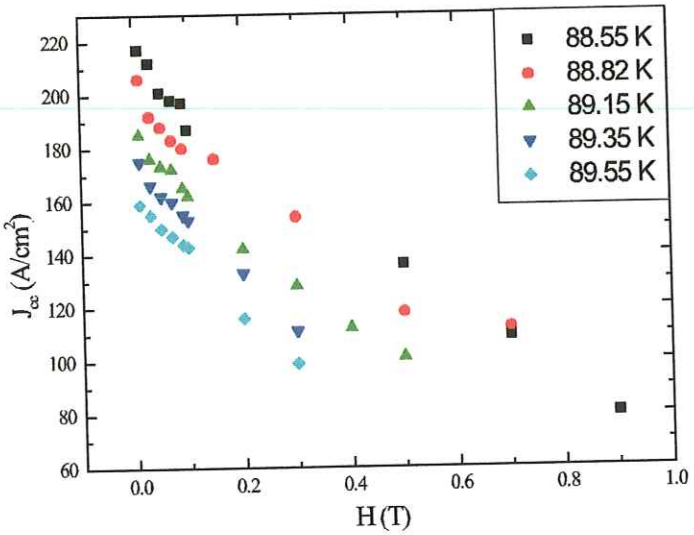

FIGURE 4.6. Most common critical current vs. magnetic field at several temperatures.

The main focus of this investigation is the critical current distributions, $f(J_c)$. These are plotted for constant temperature in figs. 4.7 - 4.11. The second derivatives were calculated using second-order Savitzky-Golay smoothing. It should be noted that some of the distributions were left out for clarity of the pictures, however, all of the CCD's followed the same basic trends. The overall shape of the CCD's is the first thing we notice. Some of the distributions appear to have one or two secondary peaks. These secondary peaks can be attributed to temperature fluctuations as can be seen by a careful analysis of the data. Although every effort was made to keep the temperature stable, the raw data shows that at every one of the secondary peaks there was a rapid temperature deviation of 0.01 to 0.02 K from the norm. The average deviation for the temperature throughout the data collection was on the order of 0.003 K.

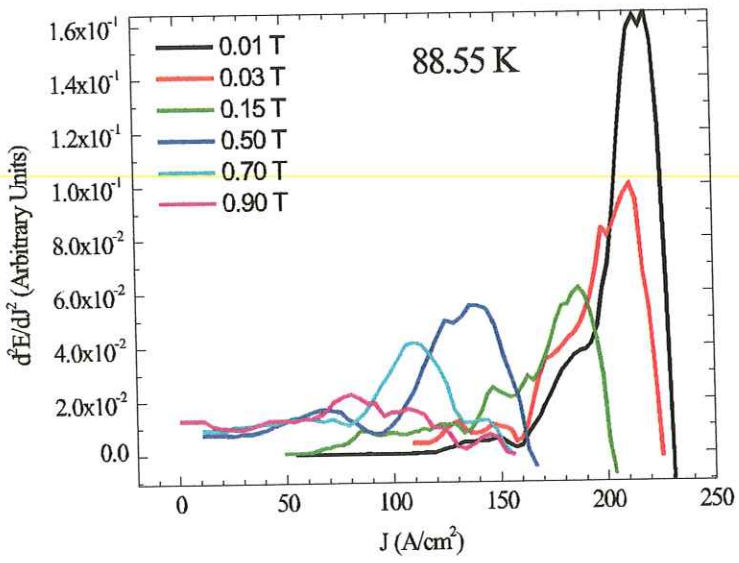

FIGURE 4.7. Critical Current Distribution at 88.55 K.

If one looks closely, however, it is clear that for smaller fields there is a small hump in every one of the distributions, just before the main peak of the curve (this is most easily noted in fig. 4.12). For larger fields this is manifest as a gentle broadening of the CCD's

on the low-current portion of the curve. This hump and broadening cannot be attributed to a temperature fluctuation. There are two possibilities which readily present themselves for the observed hump. The first is that the Co doping (at 1% substitution for Cu) is acting as a source of pinning in the sample. It has been surmised that different peaks in a CCD could be accounted for by different types of pinning [19]. Saito et al. have shown that twinning in single crystals can have a strong pinning effect [20]. Thus, a reasonable assumption would be that the peak of the CCD is due to the pinning forces of the twins. In this scenario, the Co would be increasing the pinning effect and thus increasing J_c.

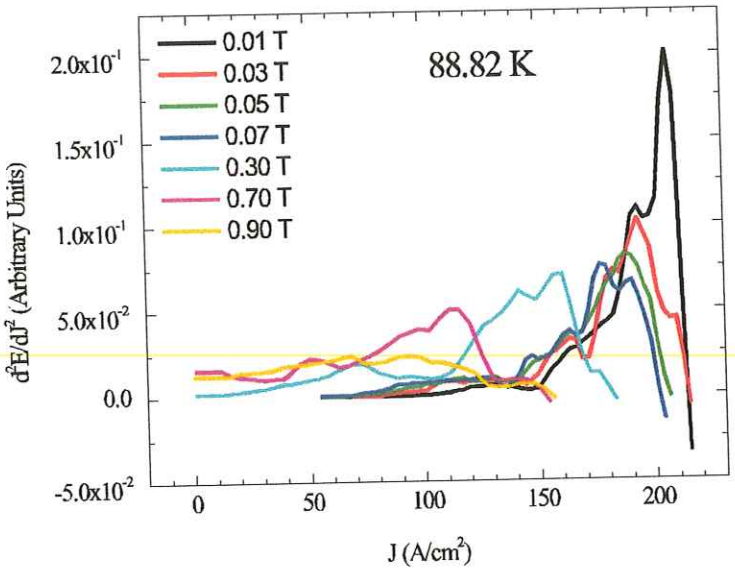

FIGURE 4.8. Critical Current Distribution at 88.82 K.

The other possibility is that the Co doping is actually decreasing the J_{cv} of the sample and broadening the CCD curve. Neiman et al. at the University of Illinois at Urbana-Champagne (where our sample was made) have shown that doping a single crystal with cobalt leads to a reduction in T_c which, by analogy to $BiSrCaCuO$, they have attributed to a decrease in the coupling between the $Cu-O$ planes [21]. If this is

so, then the decoupling should also lead to a broadening of the CCD curves, which we would observe as a small hump or broadening in our distributions.

The data presented in figure 4.12 shows the variation of the CCD's with temperature. One can see that the peak of the distribution shifts towards lower critical currents as the temperature is increased. This correlates to a decrease in the critical current of the sample. The shape of the distribution, however, remains the same.

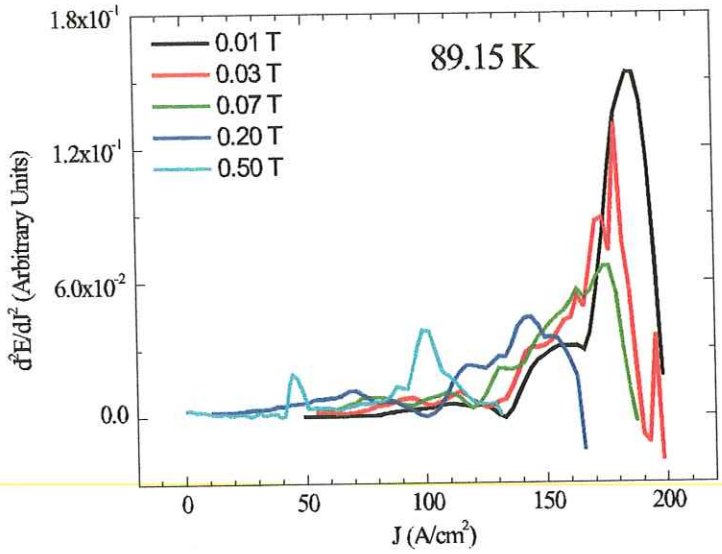

FIGURE 4.9. Critical Current Distribution at 89.15 K.

4.2. Discussion

4.2.1. Effects of Magnetic Field and Temperature

Due to the humps in the distributions it is difficult to fit the CCD's to any particular function. This makes a systematic analysis of the effects of field and temperature on the distributions rather difficult to quantify. One useful way of measuring the strength

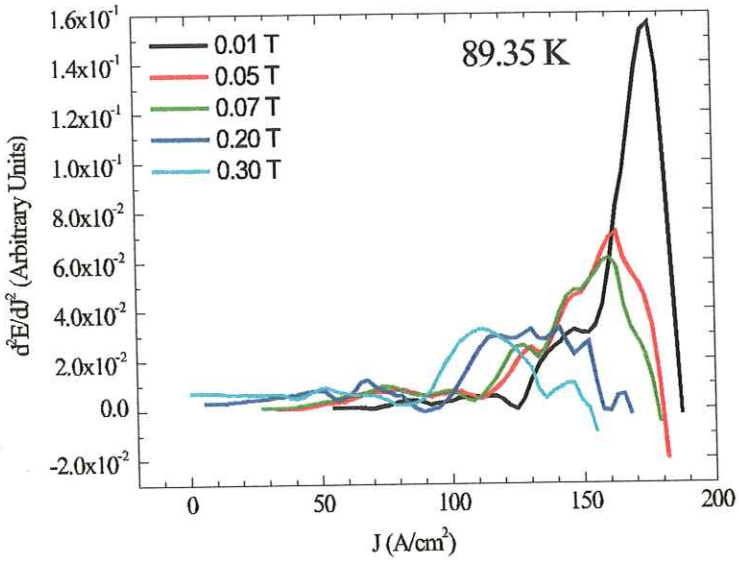

FIGURE 4.10. Critical Current Distribution at 89.35 K.

of the pinning is by plotting the average pinning force density with respect to temperature. This is calculated by multiplying the $< J_c >$ by the respective magnetic field value. Figure 4.13 shows the pinning force density vs. temperature for several fields. From this figure we see that the average pinning force decreases with increasing temperature and increases with increasing field. As the temperature increases it is expected that the effective strength of the pinning would decrease as there is more thermal energy available to help the vortices escape the pinning sites. The increase in pinning with magnetic field is expected to occur in low magnetic field regions [22]. At low fields there are fewer vortices and thus the vortex interactions are weak. As the field is increased, the motion of the individual vortices is limited by the interaction with the vortex array.

The width of the distributions is more difficult to extract from the plots of the CCD's due to the temperature fluctuations. The n-values shown in the insets of figs. 4.1 - 4.3 can be shown to correspond roughly to the steepness of the $V - I$ transition and thus

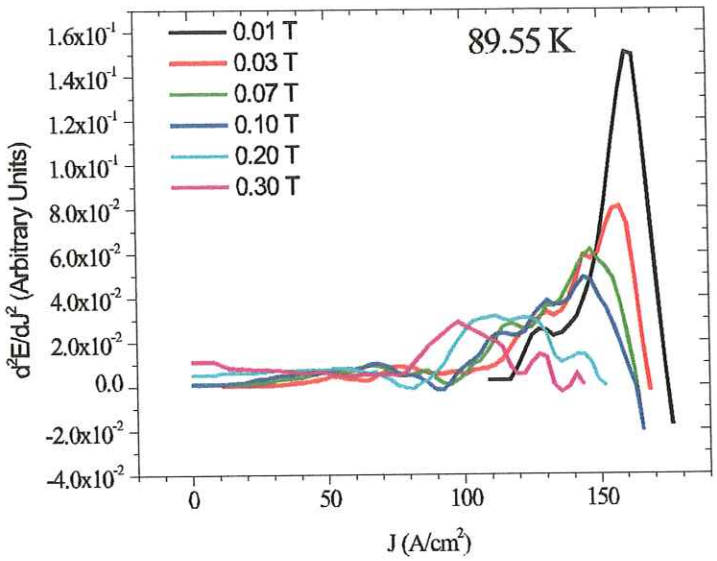

FIGURE 4.11. Critical Current Distribution at 89.55 K.

the width of the CCD's. However, it should be noted that the n-values were extracted only from the low-current portion of the curves. Thus, the width that is being measured here is the width of the left-hand side of the CCD only. From these plots it is clear that for low values of magnetic field the distributions broaden rather quickly as the field is increased. This is very similar to what Babić et al. reported in their studies on sintered ceramics. Whereas they attributed this effect to a decoupling of the superconducting grains in the ceramics, that cannot be the case here since we are dealing with a single crystal. Thus we must look for another explanation.

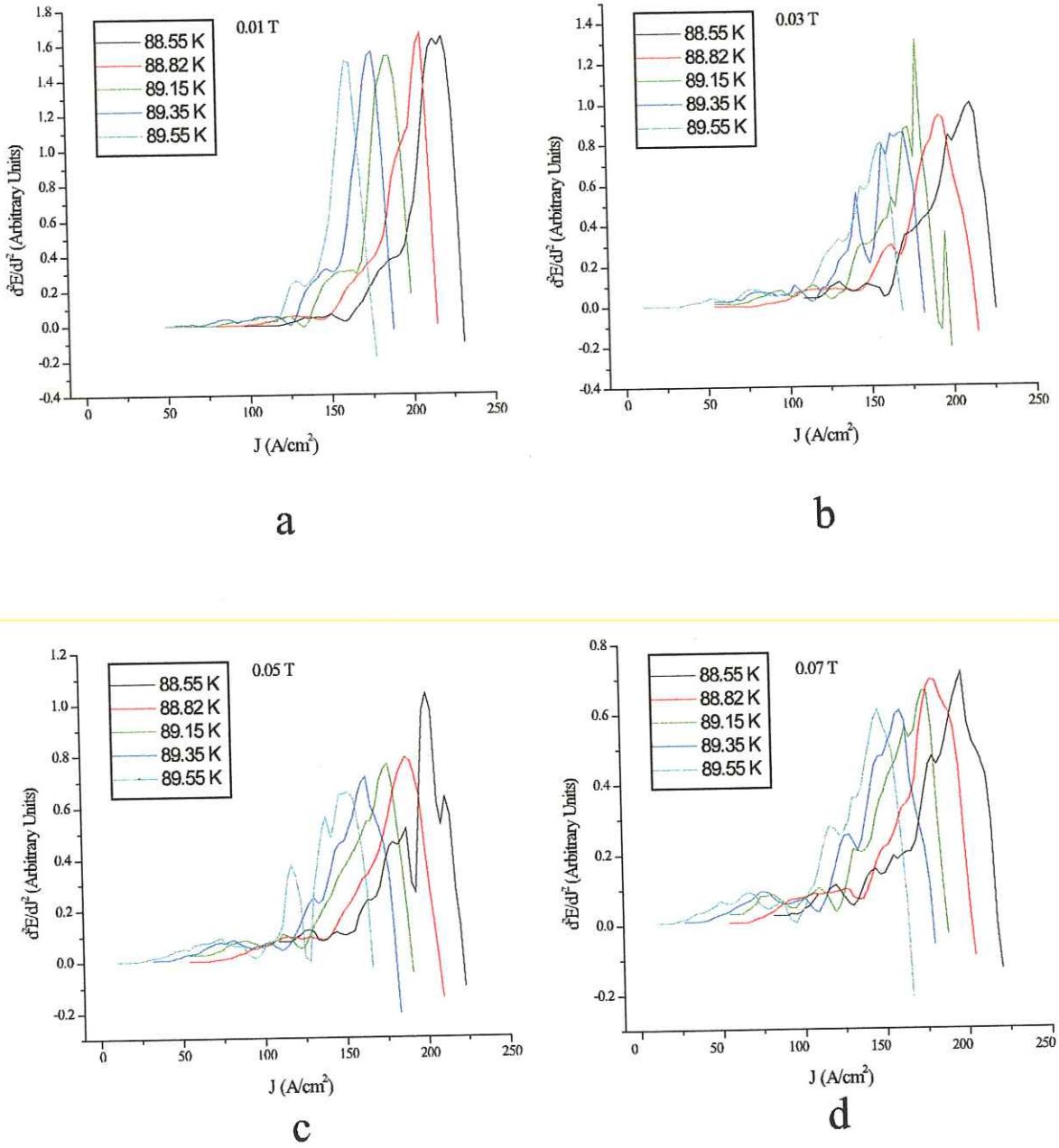

FIGURE 4.12. Critical Current Distributions at a) 0.01 T, b) 0.03 T, c) 0.05 T, d) 0.07 T.

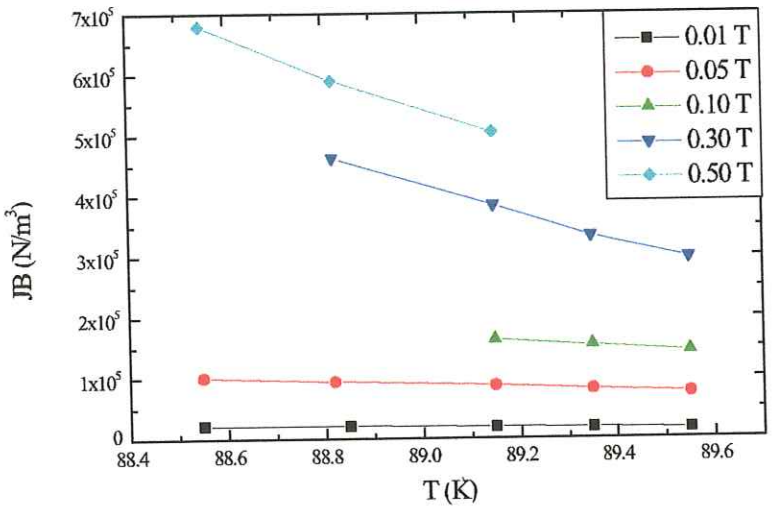

FIGURE 4.13. Force density vs. temperature for various fields

4.2.2. Effects of Cobalt Doping

It is useful to compare the results here to other studies done on sintered YBCO ceramics. Babić et al. have presented CCD curves for several sintered samples both before and after sample degradation [7]. In particular their data emphasizes three things:

- The shape of the CCD curve for the sintered samples is asymmetric, with the maximum (J_{cc}) closer to the measured J_{cv} (i.e. nearer to the low-current portion of the curve).
- As a sample deteriorates the distribution broadens and n decreases.
- After degradation the J_{cv}, as determined from the $1\ \mu V/cm$ criterion, is considerably lower, but there is little change in the maximum or the high J_c part (the tail) of the CCD.

These observations lead them to conclude that the measured J_{cv} reflects the weakest intergrain links in a sintered sample and does not reflect the overall quality. The CCD's, however, do give insight into the overall quality of a sintered sample by showing the distribution of critical currents throughout the sample.

The data presented here shows a much narrower CCD curve than that presented by Babić. The peak of the distribution is close to the maximum J_c (the point at which the $f(J_c)$ crosses the J-axis). As the magnetic field is increased the distribution widens and the peak shifts away from the high-current portion of the CCD. Although the CCD's show that the bulk of the sample has a relatively high critical current, the low-current portion has a hump and a tail which extends out to very low currents. The J_{cv}, in fact, are up to 150 A/cm^2 lower than the J_{cc}.

Brown has shown that non-Co doped samples have nearly Gaussian CCD's for low fields ($\sim$ 0.03 T) [19]. It is a reasonable assumption that twinning is the pinning force which yields the peak of the CCD's for both doped and undoped samples. If the Co were acting as a secondary pinning force it would not be expected to decrease the J_c in the sample. Rather, a strong Co pinning force would be expected to sharpen up the distribution, while a weak Co pinning force would be expected to have little effect on the CCD's as the vortices would remain pinned by the much stronger pinning forces of the twins.

It is thus more likely that the cobalt is actually serving to decrease the pinning in the sample and thus broadening the distribution. By looking at the studies done by Neiman et al. on the effects of Co doping on the irreversibility line of $YBCO$ [21] we see a possible explanation for the effect the Co is having on the CCD's. In their studies they find that at low concentrations cobalt substitutes for copper on the crystal chains. At approximately a 2.5% substitution level they see a marked changed in the functional form of the irreversibility line. By comparing this to the functional form of the irreversibility

line of $BiSrCaCuO$ and $TlBaCaCuO$ they conclude that the change could be due to a decoupling of the $Cu-O$ planes in the sample.

The sample under study in this work only has a 1% substitution of cobalt. The relatively high T_c (91.2 K) suggests that the sample is of good quality, but the J_{cv} of the sample is still rather low. It is possible that if the Co doping does have a decoupling effect on the $Cu-O$ planes that even small doses of Co would begin to weaken the coupling of the planes. If we accept Babić's conclusion that the J_{cv} measures the weakest link in a sample, then even a small amount of decoupling of the planes should lead to a reduction in the J_{cv}. The rather narrow CCD's would imply a sample of relatively high quality, while the thin tail on the low-current portion of the curve would indicate a few weak links in the sample with rather low pinning strengths.

We can now return to the field dependence of the width of the CCD. Before we noted that for low fields the distributions broaden quickly with increasing field. We can envision the effect of a small amount of decoupling of the $Cu-O$ planes by first picturing the effect of a low magnetic field. For very low fields there are very few vortices entering the superconductor. Since only the cells of the crystal with the Co substituting for the Cu actually have $Cu-O$ layers that are decoupled, few of the vortices are affected by the decoupling. Most find pinning sites away from the crystal cells with the Co and thus they are much more strongly pinned. As the magnetic field is increased, the number of vortices near the cells with decoupled layers increases, and thus the Co doping has a much stronger effect. This causes the distributions to broaden as the field is increased.

Further, the decoupling is more evident at temperatures closer to T_c, where the superconductivity is more susceptible to thermal fluctuations. This would explain why the hump disappears under the main peak at lower temperatures (see fig. 4.12).

4.2.3. Comparison to Low-T_c Superconductors

Studies of $V - I$ curves and critical current distributions in low-temperature composite superconductors proved very helpful in understanding the nature of the limitations on J_c. By looking at the variation of the parameter n with field, Warnes, et al. were able to determine whether the J_c of a sample was limited by intrinsic or extrinsic factors. If the $n - H$ plot had a steep, uniform negative slope, the composite was operating close to the intrinsic limit. If the plot was insensitive to field up to fields close to H_{c2}, and then rapidly decreased to $n = 1$, the J_c of the sample was extrinsically limited [5, 6].

By looking again at figures 4.1 - 4.3 we see that the $n - H$ plots of this sample have a very different functional form. The rapid initial decrease in n is the same field-dependence that Babić et al. see in the $n - H$ plots of the polycrystalline samples [7]. The difference in the form of the $n - H$ plots of the high-T_c and low-T_c samples probably reflects different origins of the CCD's.

The low-T_c samples also differed in that there was much more structure evident in the critical current distributions. However, the data for the composite superconductors was collected at much higher fields ($2T - 12\ T$) than the fields used in our work ($0.01 - 0.90\ T$). For this reason we do not compare our results with the results for the low-T_c samples.

4.2.4. Neutron Irradiation Studies

Neutron irradiation studies have shown that fast neutron bombardment produces a homogeneous distribution of point defects in $YBCO$ crystals. These point defects are capable of acting as flux-pinning centers and thus enhance the critical current of the crystal [23]. To our knowledge, only one study has looked at the effects of neutron irradiation on the critical current distributions of $YBCO$ [19]. Brown showed that the CCD's of

a crystal after irradiation shifted towards the higher current densities. They also began to show a double-peak structure, especially at higher magnetic fields. It was proposed that the two different peaks could be accounted for by the two different types of pinning present in the sample – twins and neutron-induced point defects. However, the study was lacking in that there was no systematic analysis of the CCD's before and after irradiation.

It would be useful to do a more comprehensive study on the effects of neutron-irradiation on single crystals of both doped and undoped $YBCO$. This kind of study would allow to compare the effects of irradiation to the effects of Co-doping to determine whether the Co is indeed reducing the J_c or is actually acting as a pinning force.

5. CONCLUSIONS

This work has investigated the distribution of critical currents in a Co-doped $YBCO$ crystal using a method originally derived for low-T_c superconductors. We have compared our results with those of Babić, who studied sintered $YBCO$ samples. The results have shown that the $E-J$ curves do yield to the conventional analysis with quite reasonable parameters. In particular we have seen that:

- The CCD's of a single crystal have a different shape than the sintered materials. In addition to having a narrower curve, the single crystal CCD's have strong high J_c content and broadening to the low J_c side of the curve. This is in contrast to the strong low J_c content and broadening to the high J_c side of the curve that Babić et al. saw.

- The CCD's of a Co-doped sample are more asymmetric than the CCD's of the non-Co-doped sample investigated by Brown. This suggests that the Co weakens the pinning, an interpretation which is supported by the work done by Ginsberg on Co-doped $YBCO$ crystals.

- The field dependence and temperature dependence of the CCD's can be explained by a decoupling of the $Cu-O$ planes induced by the cobalt doping.

As the irradiation part of the experiment was not successfully completed, we are not able to draw any conclusions about the effects of adding another source of pinning. The cobalt, however, was seen to weaken the pinning and decrease the critical current of the sample. It would be useful to compare these results to similar studies of irradiated crystals and/or crystals with varying amounts of cobalt doping.

BIBLIOGRAPHY

[1] J.G. Bednorz and K.A. Mueller. *Zeitschrift für Physik B*, 64:189, 1986.

[2] J. Baixeras and G. Fournet. *J. Phys. Chem. Solids*, 28:1541, 1967.

[3] W. Meissner and R. Oschenfeld. *Naturwisschaften*, 21:787, 1933.

[4] H. Ullmaier. *Irreversible Properties of Type II Superconductors.* Springer-Verlag, 1975.

[5] W.H. Warnes and D.C. Larbalestier. *Cryogenics*, 26:643, 1986.

[6] W.H. Warnes and D.C. Larbalestier. *Applied Physics Letters*, 20:1403, 1986.

[7] E. Babić, M. Prester, N. Biskup, Z. Marohnić, and S.A. Siddiqi. *Physical Review B*, 41:6278, 1990.

[8] H.S. Edelman and D.C. Larbalestier. *Journal of Applied Physics*, 74:3312, 1993.

[9] Q. Li, H.J. Wiesmann, M. Suenaga, L. Motowidlow, and P. Haldar. *Physical Review B*, 50:4256, 1994.

[10] A. Gurevich, A.E. Pashitski, H.S. Edelman and D.C. Larbalestier. *Applied Physics Letters*, 62:1688, 1993.

[11] M. Tinkham. *Physical Review Letters*, 61:1658, 1988.

[12] R.J. Soulen, Jr. *IEEE Transactions on Applied Superconductivity*, 3:1261, 1993.

[13] T.V. Duzer and C.W. Turner. *Principles of Superconductive Devices and Circuits.* Elsevier, 1981.

[14] G.W. Crabtreee and D.R. Nelson. *Physics Today*, 50:38, 1997.

[15] G.W. Crabtree, W.K. Kwok, U. Welp, J.A. Fendrich and B.W. Veal. *Proceedings of the International Conference on the Physics and Chemistry of Molecular and Oxide Superconductors*, 1996.

[16] E. Babić, M. Prester, D. Drobac, Z. Marohnić, P. Nozar, P. Stastny, F.C. Matacotta and S. Bernik. *Physical Review B*, 45:913, 1992.

[17] W.H. Warnes. *Journal of Applied Physics*, 63:1651, 1988.

[18] G.L. Dorofejev, A.B. Imenitov, and E.Yu. Klimenko. *Cryogenics*, 20:307, 1980.

[19] B.R. Brown. *Neutron Irradiation and dc Transport in YBaCuO Single Crystals: A Study of Vortex Depinning.* PhD thesis, Oregon State University, 1997.

[20] K.Saito, H.-U. Nissen, C. Beeli, T. Wolf, W. Schauer and H. Kupfer. *Physical Review B*, 58:6645, 1998.

[21] R. L. Neiman, J. Giapintzakis and D. M. Ginsgerg. *Physical Review B*, 54:16028, 1994.

[22] G. Blatter, M. V. Feigel'man, V. B. Geshkenbein, A. I. Larkin and V. M. Vinokur. *Review of Modern Physics*, 66:1124, 1994.

[23] F. M. Sauerzopf, H. P. Wiesinger, H. W. Weber, and G. W. Crabtree. *Physical Review B*, 54:16028, 1994.